Ultrafast X-Ray Absorption Spectroscopy of Strongly Correlated Systems: Core Hole Effect

Chen-Yen Lai and Jian-Xin Zhu
Theoretical Division, Los Alamos National Laboratory, Los Alamos, New Mexico 87545, USA
and Center for Integrated Nanotechnologies, Los Alamos National Laboratory,
Los Alamos, New Mexico 87545, USA

(Received 4 September 2018; revised manuscript received 25 April 2019; published 22 May 2019)

In recent years, ultrafast pump-probe spectroscopy has provided insightful information about the nonequilibrium dynamics of excitations in materials. In a typical experiment of time-resolved x-ray absorption spectroscopy, the systems are excited by a femtosecond laser pulse (pump pulse) followed by an x-ray probe pulse after a time delay to measure the absorption spectra of the photoexcited systems. We present a theory for nonequilibrium x-ray absorption spectroscopy in one-dimensional strongly correlated systems. The core hole created by the x ray is modeled as an additional effective potential of the core hole site, which changes the spectrum qualitatively. In equilibrium, the spectrum reveals the charge gap at half-filling and the metal-insulator transition in the presence of the core hole effect. Furthermore, a pump-probe scheme is introduced to drive the system out of equilibrium before the x-ray probe. The effects of the pump pulse with varying frequencies, shapes, and fluences are discussed for the dynamics of strongly correlated systems in and out of resonance. The spectrum indicates that the driven insulating state has a metallic droplet around the core hole. The rich structures of the nonequilibrium x-ray absorption spectrum give more insight into the dynamics of electronic structures.

DOI: 10.1103/PhysRevLett.122.207401

The primary goal of x-ray spectroscopy is to probe the properties of core level electrons and their coupling to the electrons near Fermi energy [1,2]. Contrary to the angle-resolved photoemission spectroscopy, which provides an accurate measurement of the low-energy band structure [3–6], x-ray spectroscopy offers a sensitive and versatile probe of the high-energy excitations. On the other hand, the rapidly developed resonant inelastic x-ray scattering, which is a photon-in photon-out process, provides more information on the excitation spectrum [7–10]. The short time evolution of the slightly excited initial state in both bosonic and fermionic systems can be exploited to answer fundamental questions in condensed matter physics and strongly correlated systems. In cold atom systems where the atoms have relatively slow motions [11], several studies have investigated the relaxation of the quantum state after sudden quench [12,13] and the proposed scheme to probe the properties of the many-body state [14–16]. Ultrafast laser spectroscopy provides an additional gear to investigate the electronic structure of excited states in materials. Although the photoexcited carriers usually have short lifetimes [17], the state-of-the-art pump-probe technique can still study the time evolution of the materials: for instance, cuprate superconductors [9,18,19], transition metal oxides [20,21], and charge density wave compounds [19,22–24]. Along with the development of a tabletop x-ray source [25,26], the reconstruction of the charge, spin, and lattice dynamics [27,28] from time-resolved x-ray spectroscopy is within reach. The obtained insight will be very helpful in understanding emergent phenomena in strongly correlated electron systems (among which, the Mott insulator-metal transition is one intriguing phenomenon, and the properties of excited state spectrum are difficult to measure). By using x-ray absorption in experiments [29–31], one can determine the metal-insulator transition as the temperature varies or the doping changes [18]. The dynamics of such systems, driven out of equilibrium by external stimuli, can provide insight into the underlying interactions between different coupling mechanisms within femto- to picosecond timescales [32,33]. Selective measurement techniques are necessary to probe specific excitations because the connection between various types of excitations is hidden deep in the quantum wave function, which cannot be observed directly.

Different from other probe techniques, x-ray absorption spectroscopy (XAS) also brings out the core hole effect [34–37]. Combined with the valance-electron quantum dynamics, the core hole effect is expected to create novel phenomena in nonequilibrium systems. In this Letter, we propose a single band model to study both the static and nonequilibrium (NE)-XAS of one-dimensional strongly correlated systems. We model the core hole created by the incident x ray as an attractive potential for the valence electrons [38]. In equilibrium, the spectrum reveals the metal-insulator transition for systems at the half-filling due

to the core hole effect. The NE spectra have even more features, including a metallic droplet around the core hole from a driven insulating state. Furthermore, the NE-XAS shows a resonance between the frequency of the incident pump pulse and the charge gap of the systems.

Theoretical formalism.—Starting from a conventional two-orbital model [38] and considering the dipole matrix element $\langle 3d_\sigma|T_\sigma|2p\rangle$ between two orbitals for absorption, where T_σ is a dipole transition operator, we propose an effective single band model to capture the x-ray absorption spectrum. In equilibrium, the valance electrons are described by a Fermi-Hubbard model (FHM):

$$\mathcal{H} = -J\sum_{\langle ij\rangle,\sigma}(d^\dagger_{i\sigma}d_{j\sigma} + \text{H.c.}) + U\sum_i n_{i\uparrow}n_{i\downarrow}, \quad (1)$$

where $d^\dagger_{i\sigma}$ is fermion creation operator with spin σ at site i, and the density operator is $n_{i\sigma} = d^\dagger_{i\sigma}d_{i\sigma}$. Hereafter, the hopping amplitude is set to unity $J = 1$ and the time unit is $t_0 = \hbar/J$. In general, the XAS can be determined from the Fermi golden rule

$$\mathcal{I}_{\text{XAS}}(\omega) = \sum_\sigma\sum_F |\langle F|d^\dagger_{m\sigma}|I\rangle|^2\delta(E_F - E_I - \hbar\omega). \quad (2)$$

Here, $|I\rangle$ ($|F\rangle$) and $E_{I(F)}$ are the initial (final) states and energies, and $d^\dagger_{m\sigma}$ denotes the electron excited from the core level to the valence band with spin σ at site m. Using the identity

$$\delta(x) = -\frac{1}{\pi}\lim_{\Gamma\to 0^+}\text{Im}\left\{\frac{1}{x+i\Gamma}\right\},$$

the intensity can be expressed as

$$\mathcal{I}_{\text{XAS}}(\omega) = -\frac{1}{\pi}\sum_\sigma \text{Im}\mathcal{A}_\sigma(\omega),$$

with the quantity $\mathcal{A}_\sigma(\omega)$ given by

$$\begin{aligned}\mathcal{A}_\sigma(\omega) &= -i\int_0^\infty dt e^{i\omega t}e^{-\Gamma t}\mathcal{A}_\sigma(t)\\ &= -i\int_0^\infty dt e^{i\omega t}e^{-\Gamma t}\langle I|e^{i\mathcal{H}t}d_{m\sigma}e^{-i\mathcal{H}_m t}d^\dagger_{m\sigma}|I\rangle. \quad (3)\end{aligned}$$

Here, Γ represents the core hole lifetime broadening effect. $\mathcal{H}_m$ inside the nonlocal time correlation function $\mathcal{A}(t)$ is the sum of the equilibrium Hamiltonian $\mathcal{H}$ and the effective attractive potential $-V_{\text{ch}}\sum_\sigma n_{m\sigma}$ due to the presence of the core hole. In some of the transition metal oxides, the typical core-valence interaction is about 30% stronger than the valence-valence interaction [38,53]. The initial state, $|I\rangle$, is the many-body wave function right before the x-ray probe kicks in. Below, we consider two situations: (i) the initial state as the ground state of the Hamiltonian, and (ii) a NE initial state encoding the effect of the pump pulse.

Static XAS.—In the equilibrium case, we use the ground state of Eq. (1) as the initial state, which can be obtained by a density matrix renormalization group accurately [13,54,55]. For noninteracting fermions, the wave function is a Slater determinant, which can be expressed as a matrix product state (MPS) [55,56]. Here, different initial interactions and filling fractions ($\bar{n}_f = \sum_{i\sigma}n_{i\sigma}/L$, where L is the number of lattice sites) are studied. The nonlocal time correlation function is solved in a time evolving block decimation [57–59] under the MPS framework [13,60–63]. Because the initial state is the ground state of the FHM, the evolution operator acting on the bra state can be reduced to a phase factor, i.e., $\langle\text{GS}|e^{i\mathcal{H}t} = e^{iE_{GS}t}\langle\text{GS}|$ with ground state energy E_{GS}. Due to the finite lifetime of the core hole, the simulation of real time dynamics is not required to be long to capture the spectrum quantitatively. Throughout this work, we use a time step of $\delta t = 10^{-3}t_0$ in the second order Suzuki-Trotter approximation for time evolution and a core hole lifetime of $\Gamma = 0.2J$ for calculations of the spectra.

The main objective is to capture the core hole effect in the XAS of strongly correlated systems. Starting from a noninteracting Fermi sea state at half-filling, which is shown in Fig. 1(a), the results show that the spectrum is split into two peaks from one due to the core hole potential. It is worth mentioning that the spectrum corresponds to the absorption part of the spectral density in the absence of core hole potential [38]. The locations of the peak indicate the

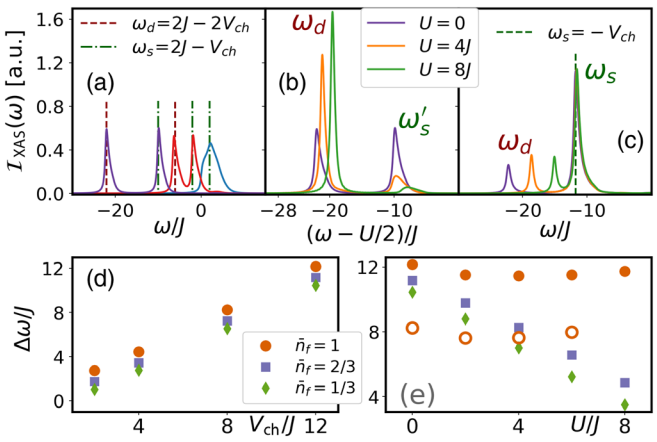

FIG. 1. Static XAS under filling fraction: (a)–(b) $\bar{n}_f = 1$, and (c) $\bar{n}_f = 2/3$. In Fig. 1(a), the initial state is the Fermi sea state ($U = 0$); and the different core hole potentials of $V_{\text{ch}}/J = 0$ (blue), 4 (red), and 12 (purple) are considered. The spectrum splits in the presence of nonzero core hole potential. In Figs. 1(b) and 1(c), with a shared legend, the initial state is the ground state with different U and the core hole potential is set to $V_{\text{ch}} = 12J$. (d) Frequency difference versus core hole potential from Fermi sea state with different fillings. (e) Frequency difference versus interaction with different fillings, where the core hole potentials are set to $V_{\text{ch}} = 12J$ (filled) and $V_{\text{ch}} = 8J$ (open).

corresponding bound state energy due to the core hole potential, which is around ω_d (ω_s) for a doubly (singly) occupied bound state at the core hole site, as marked in Fig. 1(a), where the amplitudes of both peaks are roughly the same. The difference of these two frequencies, $\Delta\omega = \omega_s - \omega_d$, reveals the core hole potential as shown in Fig. 1(d) for all three different fillings. For interacting fermions away from the half-filling, as shown in Fig. 1(c), the singly occupied state still has a stronger amplitude and all peaks are around $-V_{\mathrm{ch}}$, which signals the presence of the core hole potential. On the other hand, the doubly occupied state shifts in frequency as the interaction changes and is around $U - 2V_{\mathrm{ch}}$. This explains the energy difference of $\Delta\omega = V_{\mathrm{ch}} - U$, as shown in Fig. 1(e). Therefore, the XAS can enable us to determine the core hole potential and the interacting strength of the measured strongly correlated systems. For systems at a half-filling, three different interaction strength are compared in Fig. 1(b). In order to make a comparison to free fermions, the frequency is shifted to match the symmetric point determined by the density of states [38]. Compared to the systems away from half-filling, where only the doubly occupied state has the frequency shifted by U, both peaks are now shifted due to the strongly correlated effects. After the core electron is excited, the core hole site is nearly doubly occupied in this Mott insulating phase. Because the filling factor is exactly at half originally, the excess electron forms a doublon even if the electron escapes from the core hole site. This doublon outside the core hole site makes the frequency of the singly occupied bound state shift by U, as well as the doubly occupied bound state. Therefore, in the half-filling, the energy of the singly occupied state is shifted to $\omega_s' = U - V_{\mathrm{ch}}$ and the frequency difference is independent of the interaction as two different core hole potentials, shown in Fig. 1(e).

In addition, the weight of the corresponding response reveals important information about the electronic structure. It is defined as

$$\mathcal{W}_i = \int_{\omega_i-\delta\omega}^{\omega_i+\delta\omega} \mathcal{I}_{\mathrm{XAS}}(\omega)d\omega, \tag{4}$$

where $\delta\omega$ is a finite width that covers the decay tail due to broadening. The spectrum is normalized such that $\sum_i \mathcal{W}_i \approx 2$ due to the spin degrees of freedom. It is known that the charge gap exists in the one-dimensional half-filled FHM with any finite U in the thermodynamic limit [64,65]. From Fig. 1(b), we can immediately observe this feature. In the absence of interaction, both singly and doubly occupied bound states have almost the same weight. As the interaction increases, the weight of the doubly occupied state always dominates over the singly occupied state. We notice that the chemical potential shift is not only manifesting in the change of the dominant peak position but also in the relative intensity transfer between ω_d and ω_s peaks [66,67].

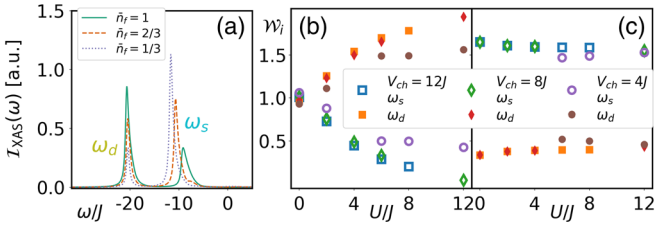

FIG. 2. (a) XAS for different fillings under the same interaction ($U = 2J$) and core hole potential ($V_{\mathrm{ch}} = 12J$). Weights of XAS from singly (open symbols) and doubly (filled symbols) occupied states: (b) $\bar{n}_f = 1$, and (c) $\bar{n}_f = 1/3$ under different interactions and core hole potentials.

Also, this weight transfer depends on the strengths of both the Hubbard interaction and the core hole potential. Figures 2(b) and 2(c) give a more quantitative analysis on the shifting weight for varying interaction strengths and core hole potentials. At the half-filling, both peaks have equal weight from the Fermi sea state, and the signals from the doubly occupied state become more dominant as the interaction becomes finite for various core hole potentials, especially in a deep core hole potential [compare the weights for $V_{\mathrm{ch}} = 4J$ and $8J$ in Fig. 2(b)]. This suggests that the charge gap opens in finite interactions. In the low electron occupation limit, the dominant signal is always the singly occupied state, as shown in Fig. 2(c). In the weak interaction regime of $U < 4J$, the weight distributions are almost identical, despite different core hole potentials.

Nonequilibrium XAS.— When there is an incident laser pulse before the x-ray photon, the initial state in Eq. (3) is no longer the ground state of the FHM. We model the effect of the laser pulse via a time-dependent Pieles phase in the Hamiltonian of $J \to Je^{iA(t)}$, where the phase has a Gaussian profile:

$$A(t) = A_0 e^{-(t+t_d)^2/2\tau^2} \cos\Omega(t + t_d),$$

with the intensity as A_0, the central frequency as Ω, the pulse shape with width as τ, and the time delay as t_d. (We set the probe as always starting at $t = 0$.) The average incoming number of photons per lattice site from the pump is estimated to be $\propto A_0^2\Omega\tau$. In order to capture the effect from the pump pulse, the time delay is chosen to be large enough where the amplitude of the pulse has almost vanished $[A(0) < 0.1]$ before measuring the XAS. Therefore, the real time dynamics of the initial ground state wave function under the pulse needs to be simulated before calculating the nonlocal time correlation function. In other words, the initial state in Eq. (3) is given by $|I\rangle = \hat{U}(-2t_d, 0)|\mathrm{GS}\rangle$, where $\hat{U}$ is the time evolution operator of the FHM, including the interaction with the electromagnetic field.

We first vary only the time delay by keeping the pulse intensity, the frequency, and the shape fixed. The NE-XAS

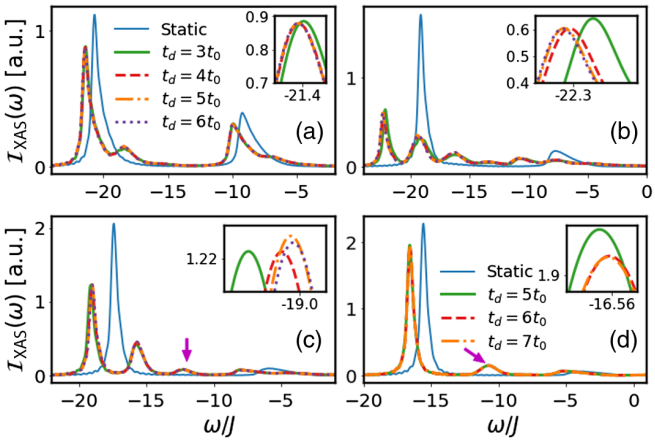

FIG. 3. NE-XAS with core hole potential $V_{\rm ch} = 12J$ and different time delays for (a) $U = 2J$, (b) $4J$, (c) $6J$, and (d) $8J$ under pulse fluences of $\Omega t_0 = 3$, $\tau = 2t_0$, and $A_0 = 0.1$ in Figs. 3(a)–3(c); and $A_0 = 0.3$ in Fig. 3(d). In Figs. 3(c) and 3(d), the peak around $\omega \sim -12J$ (magenta arrow) emerges as a singly occupied core hole signal from the metallic droplet. The system is at the half-filling.

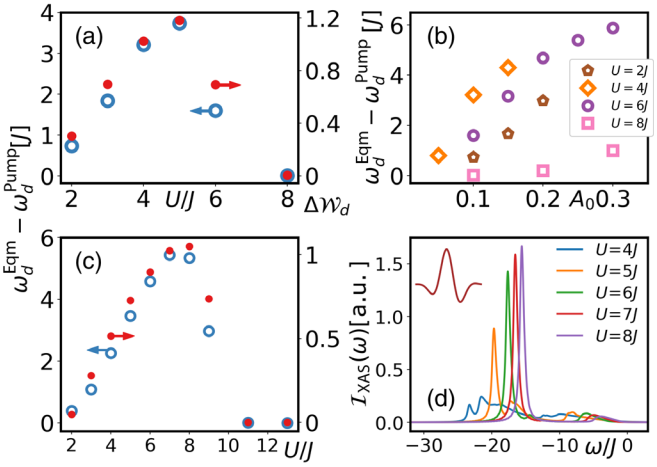

FIG. 4. (a) Changes of weight (filled symbols) and frequency (open symbols) of the doubly occupied state versus interaction under the intensity of $A_0 = 0.1$. (b) Frequency shift of the doubly occupied state versus different intensities under different interactions. In Figs. 4(a) and 4(b), the pump pulses have $\Omega t_0 = 3$, $\tau = 2t_0$, and $t_d = 6t_0$. (c) Changes of weight (filled symbols) and frequency (open symbols) of the doubly occupied state versus interaction when systems at half-filling under fluence of $\Omega t_0 = 6$, width of $\tau = 3t_0$, time delay of $t_d = 6t_0$, and $A_0 = 0.1$. (d) NE-XAS for systems at half-filling with different U under single cycle terahertz pulse fluence of $\Omega t_0 = 1$, width of $\tau = 3t_0$, time delay of $t_d = 6t_0$ and intensity of $A_0 = 1$. Inset shows the terahertz pulse profile. Core hole potential is set to $V_{\rm ch} = 12J$ in all panels.

for the half-filling is shown in Fig. 3 with different time delays t_d. Because our model does not include the relaxation effect, the NE-XAS will never recover back to the equilibrium one, even after an extended time delay. Here, the spectra from different time delays do not change much because the state only picks up some extra phases after the tail of the pulse diminishes. Small changes of the frequency and amplitude (see the insets of Fig. 3) are due to the infinitesimal tail of the pulse. As long as the time delay is long enough, the signals become translational invariant in time as one compares $t_d = 5t_0$ and $6t_0$. Also, the shifting of the peaks is roughly equal to the energy changes of the state from the pumping. Besides that, the spectrum is qualitatively different from the one at equilibrium. First of all, there are only two major peaks in the equilibrium spectrum, but the NE-XAS exhibits much richer features from the excited states. For the weak interaction case (e.g., $U = 2J$), new peaks emerge around $\omega_{d(s)} + 3J$, where the shift matches the pump pulse frequency Ω. As the interaction increases to $4J$, the fluence from the pulse is severe, and this is because the Mott gap is close to the frequency of the pump pulse. This resonance effect will be elaborated on later. Once the interaction reaches $6J$ and $8J$, a new peak emerges around $-V_{\rm ch}$. As we already mentioned, in the equilibrium spectrum, this energy corresponds to the singly occupied state (ω_s) from a metallic state. Because the photoemission spectrum shows that the system remains gapped [38], the results conjecture that this metallic signal is induced by the core hole and should be a droplet around the core hole site. A similar effect was reported in superconductors with an impurity or disorder [68].

We then vary the intensity of the pulse to study the quantitative change of the NE-XAS by using the same time delay of $t_d = 6t_0$ to ensure the pump pulse is almost finished. In Fig. 4, a quantitative analysis of the nonequilibrium XAS is shown under different shapes of the pump pulse. For all interaction strengths, both the singly and doubly occupied peaks get smaller weight as the intensity increases. One expects that the system will melt down and the spectrum will become completely featureless as the state is excited into the continuum when the pump pulse is very strong. Before that, the spectrum appears to have peaks separated by the energy close to the pump pulse frequency. It is more interesting that the pump pulse used here has a frequency of $\Omega t_0 = 3$ and the strongest influence on the $U = 5J$ state. Considering the same intensity ($A_0 = 0.1$ and 0.15, for example), the shift of the frequency of the doubly occupied state is larger for $U = 5J$, as shown in Fig. 4(b). As the interaction increases to $6J$ and $8J$, the effects of the frequency shift and the weight of the doubly occupied state are also smaller than the one of $U = 5J$, for which a detailed comparison is shown in Fig. 4(a). By switching the frequency to $\Omega t_0 = 6$, the detailed spectrum is shown in the Supplemental Material [38] and the shifting of frequency is shown in Fig. 4(c). The shift of the frequency is bigger as the interaction increases and reaches its maximum around $8J$. The effect diminishes once the interaction becomes stronger. From the results of two different frequencies, both the shift of the frequency and the change in the weight of the doubly occupied state give

the same conclusion: that there is a resonance between the pump pulse frequency and the charge gap in the systems. On the other hand, for the single cycle terahertz pulse with a frequency of $\Omega t_0 = 1$, as shown in Fig. 4(d), the results show that the spectrum becomes featureless for weak and intermediate interactions (e.g., $U \leq 4J$). As the interaction becomes stronger, the NE-XAS is less affected by the pump pulse. For instance, for $U = 8J$, the shift of the frequency and the change in weight are minimal when compared to the static XAS.

Conclusion.—We have proposed a single band model to capture the core hole effect in the XAS, and we calculated the spectrum of a one-dimensional strongly correlated system. The static XAS is able to distinguish the corresponding core hole potential and interaction strength of the strongly correlated materials. Due to the strongly correlated effect, the static XAS reveals the charge gap from the doubly occupied bound state when the system is half-filling with a finite interaction. Furthermore, considering the pump pulse with different time delays, intensities, and frequencies, the NE-XAS shows that the driven system has a metallic droplet around the core hole, which is a similar phenomenon to the impurity influence on the electronic states of superconductors. Our results have uncovered that the static and nonequilibrium XASs can help to identify the excitations contributing to the spectrum and guide the future pump-probe experiments on strongly correlated materials, such as $Sr_2CuO_{3+\delta}$ [69–71] or other cuprate compounds with a Cu-O corner (or edge) sharing chains [71–73]. Those materials can be successfully synthesized, and some of them can be doped away from the half-filling on which the photoemission spectrum has also been measured [69].

We thank Jhi-Shih You and Marton Kanász-Nagy for fruitful discussions in the early stages of this work. This work was carried out under the auspices of the U.S. Department of Energy (DOE) National Nuclear Security Administration under Contract No. 89233218CNA000001. It was supported by the Center for Integrated Nanotechnologies, which is a DOE Office of Science User Facility, and in part by the LANL LDRD Program. The numerical programs were built upon a universal tensor library [74], and the computational resources were provided by the LANL Institutional Computing Program.

[1] L. J. P. Ament, M. van Veenendaal, T. P. Devereaux, J. P. Hill, and J. van den Brink, Rev. Mod. Phys. **83**, 705 (2011).
[2] W. Olovsson, L. Weinhardt, O. Fuchs, I. Tanaka, P. Puschnig, E. Umbach, C. Heske, and C. Draxl, J. Phys. Condens. Matter **25**, 315501 (2013).
[3] A. Damascelli, Z. Hussain, and Z.-X. Shen, Rev. Mod. Phys. **75**, 473 (2003).
[4] J.-X. Zhu, A. V. Balatsky, T. P. Devereaux, Q. Si, J. Lee, K. McElroy, and J. C. Davis, Phys. Rev. B **73**, 014511 (2006).
[5] A. A. Kordyuk, Low Temp. Phys. **40**, 286 (2014).
[6] *Strongly Correlated Systems*, edited by A. Avella and F. Mancini (Springer-Verlag, Berlin, 2015).
[7] L. J. P. Ament, G. Khaliullin, and J. van den Brink, Phys. Rev. B **84**, 020403(R) (2011).
[8] M. P. M. Dean, Y. Cao, X. Liu, S. Wall, D. Zhu, R. Mankowsky, V. Thampy, X. M. Chen, J. G. Vale, D. Casa *et al.*, Nat. Mater. **15**, 601 (2016).
[9] H. Y. Huang, C. J. Jia, Z. Y. Chen, K. Wohlfeld, B. Moritz, T. P. Devereaux, W. B. Wu, J. Okamoto, W. S. Lee, M. Hashimoto *et al.*, Sci. Rep. **6**, 19657 (2016).
[10] M. Minola, G. Dellea, H. Gretarsson, Y. Y. Peng, Y. Lu, J. Porras, T. Loew, F. Yakhou, N. B. Brookes, Y. B. Huang *et al.*, Phys. Rev. Lett. **114**, 217003 (2015).
[11] C.-C. Chien, S. Peotta, and M. Di Ventra, Nat. Phys. **11**, 998 (2015).
[12] C.-Y. Lai and C.-C. Chien, Phys. Rev. Applied **5**, 034001 (2016).
[13] C.-Y. Lai and C.-C. Chien, Phys. Rev. A **96**, 033628 (2017).
[14] R. Senaratne, S. V. Rajagopal, T. Shimasaki, P. E. Dotti, K. M. Fujiwara, K. Singh, Z. A. Geiger, and D. M. Weld, Nat. Commun. **9**, 2065 (2018).
[15] A. Bohrdt, D. Greif, E. Demler, M. Knap, and F. Grusdt, Phys. Rev. B **97**, 125117 (2018).
[16] J. T. Stewart, J. P. Gaebler, and D. S. Jin, Nature (London) **454**, 744 (2008).
[17] L. Miaja-Avila, G. C. O'Neil, Y. I. Joe, B. K. Alpert, N. H. Damrauer, W. B. Doriese, S. M. Fatur, J. W. Fowler, G. C. Hilton, R. Jimenez *et al.*, Phys. Rev. X **6**, 031047 (2016).
[18] D. Fausti, R. I. Tobey, N. Dean, S. Kaiser, A. Dienst, M. C. Hoffmann, S. Pyon, T. Takayama, H. Takagi, and A. Cavalleri, Science **331**, 189 (2011).
[19] H. Matsuzaki, H. Nishioka, H. Uemura, A. Sawa, S. Sota, T. Tohyama, and H. Okamoto, Phys. Rev. B **91**, 081114(R) (2015).
[20] Y. M. Sheu, S. A. Trugman, L. Yan, C. P. Chuu, Z. Bi, Q. X. Jia, A. J. Taylor, and R. P. Prasankumar, Phys. Rev. B **88**, 020101(R) (2013).
[21] M. Gandolfi, G. L. Celardo, F. Borgonovi, G. Ferrini, A. Avella, F. Banfi, and C. Giannetti, Phys. Scr. **92**, 034004 (2017).
[22] S. Hellmann, T. Rohwer, M. Kalläne, K. Hanff, C. Sohrt, A. Stange, A. Carr, M. M. Murnane, H. C. Kapteyn, L. Kipp *et al.*, Nat. Commun. **3**, 1069 (2012).
[23] H. Yamakawa, T. Miyamoto, T. Morimoto, T. Terashige, H. Yada, N. Kida, M. Suda, H. M. Yamamoto, R. Kato, K. Miyagawa *et al.*, Nat. Mater. **16**, 1100 (2017).
[24] H. Gomi, T. Kawatani, T. J. Inagaki, and A. Takahashi, J. Phys. Soc. Jpn. **83**, 094714 (2014).
[25] J. Weisshaupt, V. Juvé, M. Holtz, S. Ku, M. Woerner, T. Elsaesser, S. Ališauskas, A. Pugzlys, and A. Baltuška, Nat. Photonics **8**, 927 (2014).
[26] D. Popmintchev, B. R. Galloway, M.-C. Chen, F. Dollar, C. A. Mancuso, A. Hankla, L. Miaja-Avila, G. O'Neil, J. M. Shaw, G. Fan *et al.*, Phys. Rev. Lett. **120**, 093002 (2018).
[27] G. Berner, M. Sing, H. Fujiwara, A. Yasui, Y. Saitoh, A. Yamasaki, Y. Nishitani, A. Sekiyama, N. Pavlenko, T. Kopp *et al.*, Phys. Rev. Lett. **110**, 247601 (2013).
[28] M. Guarise, B. D. Piazza, H. Berger, E. Giannini, T. Schmitt, H. M. Rønnow, G. A. Sawatzky, J. van den Brink,

D. Altenfeld, I. Eremin *et al.*, Nat. Commun. **5**, 5760 (2014).
[29] F. Y. Bruno, S. Valencia, R. Abrudan, Y. Dumont, C. Carrétéro, M. Bibes, and A. Barthélémy, Appl. Phys. Lett. **104**, 021920 (2014).
[30] B. Torriss, J. Margot, and M. Chaker, Sci. Rep. **7**, 40915 (2017).
[31] D. Preziosi, L. Lopez-Mir, X. Li, T. Cornelissen, J. H. Lee, F. Trier, K. Bouzehouane, S. Valencia, A. Gloter, A. Barthélémy *et al.*, Nano Lett. **18**, 2226 (2018).
[32] C. Giannetti, M. Capone, D. Fausti, M. Fabrizio, F. Parmigiani, and D. Mihailovic, Adv. Phys. **65**, 58 (2016).
[33] M. Ligges, I. Avigo, D. Golež, H. U. R. Strand, Y. Beyazit, K. Hanff, F. Diekmann, L. Stojchevska, M. Kalläne, P. Zhou *et al.*, Phys. Rev. Lett. **120**, 166401 (2018).
[34] P. J. W. Weijs, M. T. Czyżyk, J. F. van Acker, W. Speier, J. B. Goedkoop, H. van Leuken, H. J. M. Hendrix, R. A. de Groot, G. van der Laan, K. H. J. Buschow *et al.*, Phys. Rev. B **41**, 11899 (1990).
[35] V. Mauchamp, M. Jaouen, and P. Schattschneider, Phys. Rev. B **79**, 235106 (2009).
[36] C. Suzuki, T. Nishi, M. Nakada, M. Akabori, M. Hirata, and Y. Kaji, J. Phys. Chem. Solids **73**, 209 (2012).
[37] J. C. Fuggle and N. Mårtensson, J. Electron Spectrosc. Relat. Phenom. **21**, 275 (1980).
[38] See Supplemental Material at http://link.aps.org/supplemental/10.1103/PhysRevLett.122.207401 for the derivation of effective single band model, the photoemission spectroscopy, and the NE-XAS for different frequency and systems away from half-filling, which includes Refs. [39–52].
[39] A. Nocera, U. Kumar, N. Kaushal, G. Alvarez, E. Dagotto, and S. Johnston, Sci. Rep. **8**, 11080 (2018).
[40] D. Benjamin, I. Klich, and E. Demler, Phys. Rev. Lett. **112**, 247002 (2014).
[41] C. Jia, K. Wohlfeld, Y. Wang, B. Moritz, and T. P. Devereaux, Phys. Rev. X **6**, 021020 (2016).
[42] M. Kanász-Nagy, Y. Shi, I. Klich, and E. A. Demler, Phys. Rev. B **94**, 165127 (2016).
[43] E. Jeckelmann, Phys. Rev. B **66**, 045114 (2002).
[44] T. D. Kühner and S. R. White, Phys. Rev. B **60**, 335 (1999).
[45] K. A. Hallberg, Adv. Phys. **55**, 477 (2006).
[46] H. Benthien, F. Gebhard, and E. Jeckelmann, Phys. Rev. Lett. **92**, 256401 (2004).
[47] M. Ganahl, M. Aichhorn, H. G. Evertz, P. Thunström, K. Held, and F. Verstraete, Phys. Rev. B **92**, 155132 (2015).
[48] F. Carbone, D.-S. Yang, E. Giannini, and A. H. Zewail, Proc. Natl. Acad. Sci. U.S.A. **105**, 20161 (2008).
[49] C. Kim, Z.-X. Shen, N. Motoyama, H. Eisaki, S. Uchida, T. Tohyama, and S. Maekawa, Phys. Rev. B **56**, 15589 (1997).
[50] C. Kim, A. Y. Matsuura, Z.-X. Shen, N. Motoyama, H. Eisaki, S. Uchida, T. Tohyama, and S. Maekawa, Phys. Rev. Lett. **77**, 4054 (1996).
[51] G. Barcza, O. Legeza, F. Gebhard, and R. M. Noack, Phys. Rev. B **81**, 045103 (2010).
[52] G. Barcza, W. Barford, F. Gebhard, and O. Legeza, Phys. Rev. B **87**, 245116 (2013).
[53] A. Hariki, T. Uozumi, and J. Kuneš, Phys. Rev. B **96**, 045111 (2017).
[54] S. R. White, Phys. Rev. Lett. **69**, 2863 (1992).
[55] U. Schollwöck, Ann. Phys. (Amsterdam) **326**, 96 (2011).
[56] P. Silvi, D. Rossini, R. Fazio, G. E. Santoro, and V. Giovannetti, Int. J. Mod. Phys. B **27**, 1345029 (2013).
[57] G. Vidal, Phys. Rev. Lett. **91**, 147902 (2003).
[58] G. Vidal, Phys. Rev. Lett. **93**, 040502 (2004).
[59] A. E. Feiguin and S. R. White, Phys. Rev. B **72**, 020404(R) (2005).
[60] A. J. Daley, C. Kollath, U. Schollwöck, and G. Vidal, J. Stat. Mech. (2004) P04005.
[61] I. P. McCulloch, J. Stat. Mech. (2007) P10014.
[62] C.-Y. Lai, J.-T. Hung, C.-Y. Mou, and P. Chen, Phys. Rev. B **77**, 205419 (2008).
[63] C.-Y. Lai and C.-C. Chien, Sci. Rep. **6**, 37256 (2016).
[64] E. H. Lieb and F. Y. Wu, Phys. Rev. Lett. **20**, 1445 (1968).
[65] E. H. Lieb and F. Y. Wu, Physica (Amsterdam) **321A**, 1 (2003).
[66] P. A. van Aken and B. Liebscher, Phys. Chem. Miner. **29**, 188 (2002).
[67] H. Tan, J. Verbeeck, A. Abakumov, and G. Van Tendeloo, Ultramicroscopy **116**, 24 (2012).
[68] A. V. Balatsky, I. Vekhter, and J.-X. Zhu, Rev. Mod. Phys. **78**, 373 (2006).
[69] T. E. Kidd, T. Valla, P. D. Johnson, K. W. Kim, G. D. Gu, and C. C. Homes, Phys. Rev. B **77**, 054503 (2008).
[70] A. Keren, L. P. Le, G. M. Luke, B. J. Sternlieb, W. D. Wu, Y. J. Uemura, S. Tajima, and S. Uchida, Phys. Rev. B **48**, 12926 (1993).
[71] N. Motoyama, H. Eisaki, and S. Uchida, Phys. Rev. Lett. **76**, 3212 (1996).
[72] M. Hase, I. Terasaki, and K. Uchinokura, Phys. Rev. Lett. **70**, 3651 (1993).
[73] B. J. Kim, H. Koh, E. Rotenberg, S.-J. Oh, H. Eisaki, N. Motoyama, S. Uchida, T. Tohyama, S. Maekawa, Z.-X. Shen *et al.*, Nat. Phys. **2**, 397 (2006).
[74] Y. J. Kao, Y. D. Hsieh, and P. Chen, J. Phys. Conf. Ser. **640**, 012040 (2015).